ELSEVIER

J. Non-Newtonian Fluid Mech. 135 (2006) 97–108

Journal of Non-Newtonian Fluid Mechanics

www.elsevier.com/locate/jnnfm

Impact dynamics of a solid sphere falling into a viscoelastic micellar fluid

Benjamin Akers[1], Andrew Belmonte*

The W.G. Pritchard Laboratories, Department of Mathematics, Pennsylvania State University, University Park, PA 16802, USA

Received 22 February 2005; received in revised form 14 December 2005; accepted 20 January 2006

Abstract

We present an experimental study of the impact of a solid sphere on the free surface of a viscoelastic wormlike micellar fluid. Spheres of various densities and diameters are dropped from different heights above the fluid surface, reaching it with a nonzero velocity which determines the subsequent dynamics. Measurements of the initial sphere penetration are found to scale with the ratio of the kinetic energy of the sphere at impact to the elastic modulus of the fluid. The cavity formed in the wake of the sphere, observed with high-speed video imaging, also undergoes transitions from a smooth to fractured surface texture, dependent on both the Deborah number and the ratio of the gravitational force to elasticity.

Keywords: Impact; Sedimentation; Splashing; Free surface flows; Wormlike micelles; Cavity pinch-off; Fracture

1. Introduction

The impact of a solid on the free surface of a fluid is a ubiquitous problem arising in areas as diverse as military projectiles [1] and water-walking lizards [2]. The fundamental phenomenon involves the cavity and/or splash produced by the object as it enters the fluid, often accompanied by bubble entrainment and acoustic noise [3,4]. If the object has a spatial dimension d, and is moving at velocity U_0 when it reaches the surface, the relevant non-dimensional number characterizing the ensuing phenomena is the Froude number

$$Fr = \frac{U_0^2}{gd},$$

where g is the gravitational acceleration [1,2,5,6]. For instance, the air cavity entrained by the object closes off first near the original surface for approximately $Fr < 70$ (known as surface closure), whereas it closes near its midpoint (deep closure) for roughly $Fr > 150$ [1,7]. A coin dropped a few inches above a glass of water forms a cavity,[2] and corresponds to $Fr \sim 5$; an equivalent case appears in Fig. 5b of [2].

We are concerned here with the impact of a solid sphere on the surface of a viscoelastic fluid, a fluid which combines aspects of an elastic solid and a fluid. If the fluid is Newtonian and viscous effects dominate (i.e. the Reynolds number $Re \ll 1$), then the drag forces will come into balance with gravity, and a steady terminal velocity will be reached [8,9]. In a viscoelastic fluid, it is well known that the transient velocity can exhibit oscillations while approaching this steady state [10]. Recently a class of viscoelastic fluids has been identified for which sinking spheres do not reach a steady terminal velocity, due perhaps to breaking events on the microscopic scale; this includes both wormlike micellar fluids [11,12] and associating polymer networks [13,14]. Similarly, rising bubbles also oscillate in wormlike micellar fluids [15] with a sensitive dependence on temperature and concentration [16]. This dependence derives from the nature of wormlike micellar fluids, which owe their elasticity to long tubelike aggregates of surfactant molecules [17].

In this paper we study sphere impact on the free surface of a wormlike micellar fluid. By varying the sphere size and density, as well as the drop height, we characterize the sphere dynamics, cavity shape, and pinch-off in terms of the relevant non-dimensional parameters. We also study the transition from smooth to rough cavity surface. This work is in some sense a continuation of our studies of surface folds and buckling for a sinking sphere starting with zero velocity at the surface [18,19].

* Corresponding author.
E-mail address: belmonte@math.psu.edu (A. Belmonte).
[1] Present address: Department of Mathematics, University of Wisconsin, Madison, WI, USA
[2] The formation of the cavity for a freely falling coin depends to some extent on the angle with which the coin enters the water.

0377-0257/$ – see front matter © 2006 Elsevier B.V. All rights reserved.
doi:10.1016/j.jnnfm.2006.01.004

2. Background

When a fluid drop or solid object falls through a free fluid surface, a common occurrence is the appearance of a tall fluid jet rising upwards. This 'Worthington jet' can extend several meters above the surface, depending on the fluid parameters [20]. Typical studies of impact phenomena, whether focusing on the flow above or below the original quiescent surface (splash or cavity), have been concerned with high speeds, which translates into high fluid inertia (high *Re*) [1,20].

We leave aside the considerable literature on this well-studied subject, and focus on the different kinds of splashes which occur in viscoelastic fluid and other complex materials: much less has been done for this case. Walters and coworkers have performed a series of studies focusing on the differences between Newtonian and non-Newtonian (viscoelastic) fluids in the free-surface impact of a solid [21–23]. The first two studies focused on the dramatic reduction in the height of the Worthington jet with the addition of a small amount of polymer. These studies used the impact of a solid sphere or a fluid drop, comparing viscous Newtonian and non-Newtonian fluids while focusing mainly on the fluid dynamics above the surface. In a subsequent study, Nigen and Walters [23] also observed the cavity shape and depth at pinch-off for polymer fluids, this time comparing sphere impact to the impact of solid cylinders and rings (for $Fr \sim 10$–100). The cavity shapes they observed are similar to Newtonian fluids, and in many ways different than the observations reported here.

The impact of a solid object into a granular material resembles the impact on a fluid in a surprising number of ways. One obvious difference is that the asymptotic state in a fluid is that the object sinks, whereas in granular material the object ends up embedded and stationary. Yet there are a number of similarities between impact on granular and fluid surfaces, including a jet-like splash [24,25], a collapsing cavity [25], and a complex stress dynamics during the splash [26]. Recently this analogy was carried over to the modeling of a granular material as a non-Newtonian fluid [27].

Other studies with some similarities to our work are the impact of a solid sphere on a fluid density gradient [28,29], in which transient sphere oscillations are also seen. These oscillations are due not to fluid elasticity, but to the overshoot of the sphere past its neutrally buoyant level, and also the buoyant restoring force of fluid entrained against the density gradient. There are also many studies of surface impact and cavity dynamics due to a drop or liquid column striking a free Newtonian fluid surface; see e.g. [30,31].

Three recent experimental studies have addressed some aspect of impact in wormlike micellar fluids [32–34]. The closest to our work is the brief study by Wang et al. of splashes produced by the impact of a solid sphere into various wormlike micellar fluids [32]. This study, which was motivated by the work of the Walters group, focused exclusively on the reduction in height of the Worthington jet for micellar fluids known to be turbulent drag reducting agents, and found an interesting sensitivity to the chain length of the surfactant tails [32]. Another study focused on the impact and recoil of a liquid drop of wormlike micellar fluid on a hydrophobic surface [33]. Very recently, a combined rheological and hydrodynamic study was performed on the impact of a water drop into a shallow layer of wormlike micellar fluid, focusing on the crown development in the splash for various concentrations [34].

3. Experimental setup

The experimental fluid used is an aqueous solution of the wormlike micellar system cetylpyridinium chloride (CPCl)/sodium salicylate (NaSal), in which the organic salt NaSal facilitates the formation of long tubular "wormlike" surfactant micelles [35–37]. The CPCl and NaSal used here are obtained from Aldrich, and dissolved in filtered deionized water without further purification. The fluids were mixed for several days, then allowed to sit for a day before use. We use a viscoelastic solution of 80 mM CPCl and 60 mM NaSal, similar to a standard mixture of 100 mM CPCl/60 mM NaSal [35,37]. The density of our fluid was measured to be $\rho_f = 1.0\,\mathrm{g/cm^3}$. The rheological properties were measured previously in a temperature controlled couette cell rheometer [38]; the fluid was found to be shear thinning, with a zero shear viscosity $\eta_0 \simeq 430\,\mathrm{P}$, a relaxation time $\lambda \simeq 2\,\mathrm{s}$, and an elastic modulus $G_0 \simeq 220\,\mathrm{dyn/cm^2}$.

For a viscoelastic fluid comprised of surfactant aggregates, one would expect the relevant surface tension to depend on the timescale of the dynamic processes. An equilibrium surface tension of 36 mN/m has been measured for several different concentrations of equimolar CTAB/NaSal [15,33]. However it was also shown by Cooper-White et al. that dynamic surface tension effects can be important; for equimolar CTAB/NaSal solutions in the range 1–10 mM, the surface tension can be as high as that of pure water if the timescale of the motion is shorter than about 15 ms [33]. At longer timescales the measured surface tension is lower, and approaches its equilibrium value for timescales around 1 s [33]. In the absence any surface tension measurements in the literature for the CPCl/NaSal system, we used the pendant drop technique [39] to measure the equilibrium surface tension between 80 mM CPCl/60 mM NaSal and air; our measured value of 32 ± 2 mN/m is not far from the equilibrium value for low concentration CTAB/NaSal [15,33]. However, as the typical timescales of sphere impact in our experiment can be quite rapid, a surface tension γ closer to 70 mN/m (water) would probably be more appropriate.

Experiments were performed with a variety of spheres, with different densities ρ_s (1.4–8.0 g/cm^3) and diameters d (1.0–2.5 cm); experimental parameters are listed in Table 1. The spheres were initially dry before being dropped into the fluid, and were not roughened before use. We therefore consider the spheres to be smooth—despite using a variety of materials we did not see any systematic dependence on the minor variation in smoothness between spheres, such as between glass and teflon. The fluid was contained in one of two different large plexiglass cylinders, with diameters $D = 14.6$ and 24.2 cm, and total fluid depths $H = 25$ and 46 cm, respectively. The experiments were performed at a room temperature of 20–21 °C, and the cylinder was placed in a large water-filled rectangular glass tank for temperature stabilization, and to eliminate the optical distortion

Table 1
Material properties relevant to our experiments on sphere impact into a wormlike micellar fluid, including the range of *Re*, *De*, and *Fr* based on the speed at the moment the sphere reaches the surface; h_0 is the drop height, "steel" is type 316 stainless steel, and SiNi stands for silicon nitride. The parameter *Fe* is the elastic Froude number (Eq. (1))

Sphere	ρ_s (g/cm^3)	d (cm)	h_0 (cm)	*Re*	*De*	*Fr*	*Fe*
Delrin	1.35	1.27 (1/2 in.)	3–10	0.2–0.7	120–380	5–47	9–95
Delrin	1.35	2.54 (1 in.)	5–50	0.6–1.9	78–250	4–40	15–155
Teflon	2.17	1.27 (1/2 in.)	5–90	0.3–1.2	155–660	8–142	50–940
Teflon	2.17	1.9 (3/4 in.)	10–30	0.6–1.1	145–255	10–32	100–320
Glass	2.61	1.27 (1/2 in.)	5–40	0.3–0.8	155–440	8–63	70–575
SiNi	3.19	0.953 (3/8 in.)	0.5–127	0.1–1.1	65–1050	1–270	10–2480
SiNi	3.19	1.27 (1/2 in.)	5–90	0.3–1.2	155–660	8–140	100–1760
Steel	7.97	0.953 (3/8 in.)	5–70	0.2–0.8	210–780	10–150	310–4350
Steel	7.97	1.27 (1/2 in.)	5–40	0.3–0.8	155–440	8–65	310–2485

of the curved cylinder walls. The time dynamics of the falling sphere were recorded using a high-speed digital video camera (Phantom v5.0), capable of capturing up to 60,000 frames per second (fps); typical rates in our study were 500–1000 fps. The images were transferred and stored on a desktop computer for analysis. The depths of the sphere were measured by lining up the digital crosshairs in an image analysis program with the leading edge of the sphere, and converting this pixel measurement to true distance.

The falling sphere was always dropped into the center of the cylindrical cell, and thus during the initial penetration of the sphere the walls were always sufficiently far away ($d/D \leq 1/50$) to be unimportant. The absence of wall effects was directly confirmed in a separate series of experiments, in which we took advantage of the fluid state just after it has been poured into the cylinder. Before the fluid has had time to clear, it contains a quasi-uniform distribution of small bubbles which act as flow tracers. By dropping a sphere into this fluid, we could observe the maximum radius of fluid disturbance as a function of time, which has not yet reached the cylinder walls before the sphere stops at its initial penetration depth. The disturbance does, however, reach the walls (and reflect back from them) *before* the first rebound height is reached, affecting the subsequent sphere dynamics, as discussed below.

Assuming that the velocity of the sphere at the fluid surface is given by the potential energy it had at the height h_0 from which it was dropped, we can write the initial velocity as $U_0 = \sqrt{2gh_0}$ [23]. From this we define the standard non-dimensional numbers characterizing the surface impact flow: the Reynolds, Deborah, and Weber numbers

$$Re = \frac{\rho_f U_0 d}{\eta_0}, \qquad De = \frac{\lambda U_0}{d}, \qquad Wb = \frac{\rho_f U_0^2 d}{\gamma}.$$

For our experiments, $Re \sim 10^{-2}$ to 1, and $De \sim$ 10–800 (see Table 1). Based on the surface tension of water (see discussion above), $Wb \sim$ 13–3400.

4. Sphere trajectory during impact

Using this strongly viscoelastic wormlike micellar fluid, we studied experimentally the dynamics of a falling rigid sphere, and the cavity which it forms, as a function of sphere size, density, and entry speed. For comparison we briefly summarize qualitative observations performed in some standard Newtonian fluids (pure water, and a glycerol/water mixture): (1) the sphere forms a cavity as it enters the fluid; (2) the cavity seals, entraining some air; (3) the sphere continues to sink, though at a slower rate, and eventually reaches a steady-state velocity. This is essentially the scenario which has been observed previously [40].

Here we focus mainly on two additional phenomena which occur in the non-Newtonian case. One is the well-known fact that the sphere exhibits transient oscillations [10,41], due to the elasticity of the fluid. The second is a roughness transition on the surface of the cavity, where the fluid appears to be tearing, more like a solid.

4.1. Experimental observations

The typical sequence of events occurring during sphere impact on a wormlike micellar fluid is summarized in Fig. 1 for a $d = 0.95$ cm silicone nitride sphere dropped from $h_0 = 30$ cm. The sphere initially plunges rapidly into the fluid (Fig. 1a), then slows as it sinks until being stopped by the fluid elasticity (Fig. 1b). The sphere is then pulled back upwards, as if by a rubber-band (Fig. 1c–e), similar to the oscillatory transient seen when a sphere falls from rest within a viscoelastic polymer fluid [10,41]. The sphere rises to some height (Fig. 1f) before gravity eventually pulls it back downward again. Sometime between the initial impact and the first velocity reversal (Fig. 1a and b), the air cavity drawn out behind the sphere closes.

In Fig. 2, the position of the leading edge of the sphere is plotted as a function of time, clearly showing the oscillations of the sphere as it sinks. In our experiments we focus on two aspects of this curve: (1) the initial depth which the sphere reaches before elastic forces stop its progress, and the sphere velocity $U = 0$, which we call *the penetration depth* z_p; and (2) the subsequent position z_R to which the sphere bounces upwards before it again starts a downward descent. There are usually a few more oscillations before the sphere settles into a steady sinking rate. Additionally we study the cavity formed by the sphere when it enters the micellar fluid, focusing on the distance below the surface at which the cavity pinches off (the seal depth z_s, see e.g. Gaudet [6]), and the visible changes in the cavity surface texture.

In general the penetration depth z_p should depend on the sphere diameter d, density ρ_s, and the initial drop height h_0.

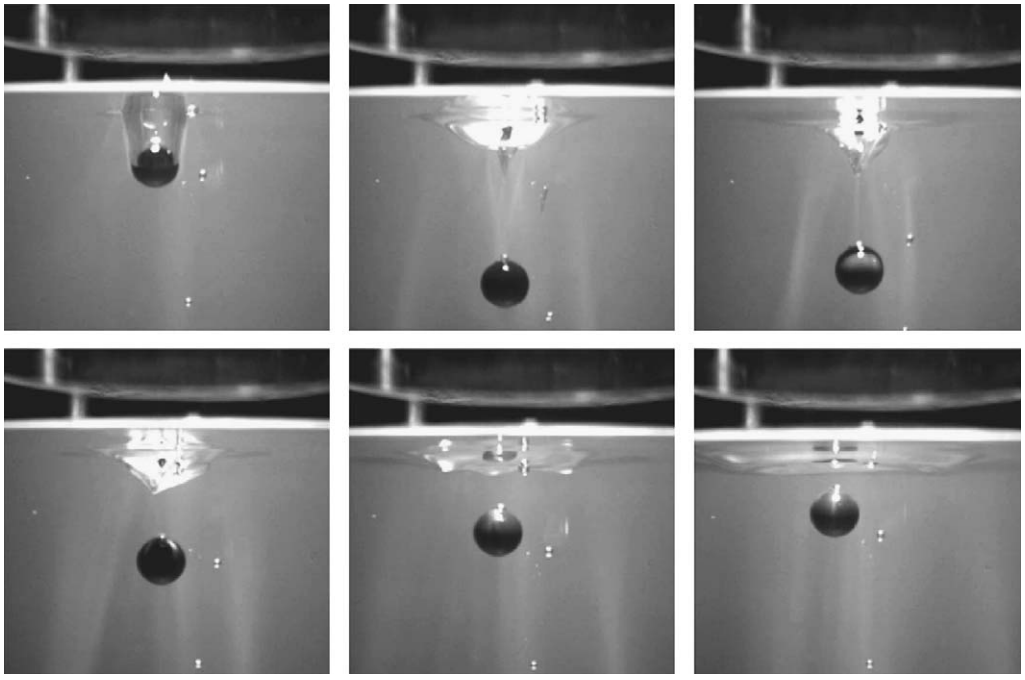

Fig. 1. Sequential images of the penetration of a 0.95 cm diameter silicone nitride sphere dropped from $h_0 = 30$ cm into 80/60 mM CPCl/NaSal solution ($Re \simeq 0.5$, $Fr \simeq 60$, $Fe \simeq 590$). The time between images is 40 ms.

As one might expect, z_p increases with h_0, as shown in Fig. 3 for different spheres. This is reasonable, as a greater initial kinetic energy allows the sphere to penetrate further before being stopped by the elastic restoring force inherent in the micellar fluid. One might expect an asymptote in this dependence: a kinetic energy above which the fluid elasticity is unable to stop the sphere at any moment, determined by the maximum storable energy in the wake. However, we have not reached such a regime in our experiments. The dependence of z_p on the drop height h_0 appears roughly linear for each sphere (Fig. 3), though some curvature is evident near the origin for some of the data. This is as one would expect, since for $h_0 = 0$ there will be no initial velocity, which should lead to $z_p = 0$. Note also that there is apparently a different curve for each sphere.

Historically, the standard dimensionless scaling for the impact of a solid object into a Newtonian fluid involves the Froude

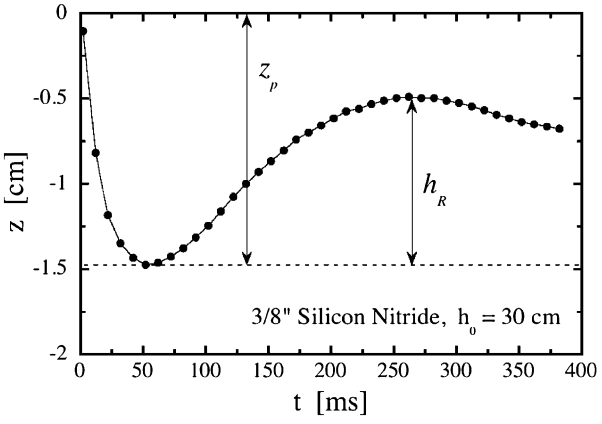

Fig. 2. The dynamics after impact (depth z vs. time) of a silicon nitride sphere, $d = 0.95$ cm, $h_0 = 30$ cm (same experiment as Fig. 1).

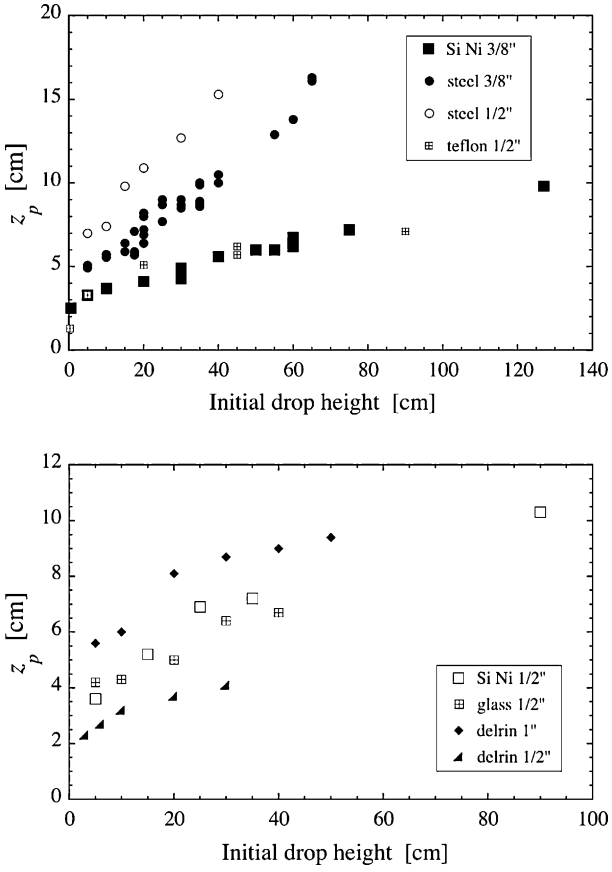

Fig. 3. Dependence of the penetration depth z_p on the initial drop height h_0 for several different spheres in our experiment.

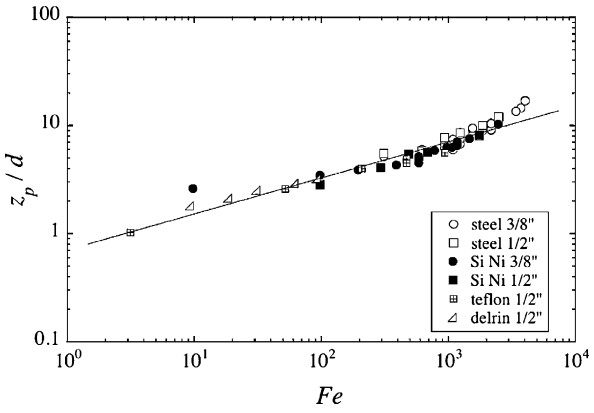

Fig. 4. Non-dimensional plot of the penetration depth z_p/d vs. the elastic Froude number Fe (see text) for six different data sets. The straight line corresponds to the scaling law $z_p/d \sim Fe^{1/3}$.

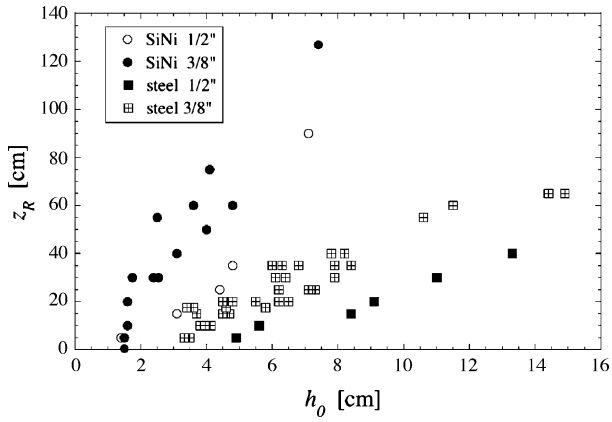

Fig. 5. Dependence of the position of the first rebound z_R on the initial drop height h_0 for several different spheres in our experiment.

number, denoted Fr [1,2,6]. However this scaling does not work with the penetration depth data z_p shown in Fig. 3, due primarily to the elasticity of the micellar fluid. Instead, we find that the normalized values z_p/d will collapse onto a single curve if plotted against the following non-dimensional ratio

$$Fe = \frac{\Delta\rho U_0^2}{G} = Fr\frac{\Delta\rho g d}{G}, \tag{1}$$

where $\Delta\rho = \rho_s - \rho_f$, and G is the elastic modulus of the fluid. We will refer to Fe as the *elastic Froude number*. This number is essentially the square of Joseph's elastic Mach number [42], which is the ratio of the fluid velocity U_0 to the elastic wave speed $\sqrt{G/\rho_s}$. It is also the product of the Deborah and Reynolds numbers with the normalized density difference,

$$\left(\frac{\Delta\rho}{\rho_f}\right) De\, Re = \frac{\Delta\rho U_0^2 \lambda}{\eta_0} = \frac{\Delta\rho U_0^2}{G} = Fe$$

note that Fe is not the same as the "elasticity number" $E = De/Re$ [9]. By replotting our data as the normalized depth z_p/d against Fe, we find that all points collapse onto a single curve, with overall scaling $z_p/d \sim Fe^{1/3}$, as shown in Fig. 4. An argument leading to this scaling exponent is given in Section 6.

We have also measured the position of the first rebound z_R of the sphere, the next point at which the velocity U is zero. The well-known phenomenon of sphere rebound in viscoelastic fluids [10,41] occurs because the microscopic constituents responsible for the elasticity (such as polymers, or as here micellar tubes), which were stretched along the trajectory as the sphere plunged into the fluid, exert an opposing force which works to pull the sphere back upwards. Some examples of the dependence of the first rebound position on initial drop height are shown in Fig. 5. While the trend in the data – that z_R increases with h_0 – seems to imply that there is a greater rebound for a larger drop height (larger U_0), this is in fact only an artifact due to the fact that z_R is defined as the absolute position to which the sphere rebounds, not the distance it covers. We therefore define *the rebound height* $h_R = z_p - z_R$ (see Fig. 2), and replot this data in Fig. 6. What is most striking about the rebound height h_R is its approximate independence of the density or size of the sphere, or even the drop height h_0, which means that h_R does not even depend on U_0; in most cases the spheres rebound about 2.5 cm.

We first no that there is much more scatter in this plot, indicative of the sensitivity of the rebounding sphere to fluctuations in the fluid. The independence of this quantity of any of the varied parameters, such as sphere density, diameter, or Re, Fr, or Fe, suggests that it is being determined by something else, such as the container itself. In fact, there is evidence from flow visualization (discussed above) that the flow has reaches the cylinder walls. Thus it may be that the rebound dynamics are dominated by a sort of resonance of the container, as was strikingly seen in shear-thinning polymer fluids [10]; birefringent visualization in other wormlike micellar systems also support this conjecture [44].

The additional time needed for the sphere to rebound upwards allows for other factors to enter into the problem, increasing its complexity. For instance, the cylindrical container may now play a role, as disturbances have had time to reach the walls and return to the sphere. Another complicating factor for the rebound comes from the fact that the sphere is now moving backwards into its own wake. There is much evidence that spheres falling through wormlike micellar fluids produce flow-induced structures (FIS) in their wake [11,12]; the same is true of rising bubbles [16].

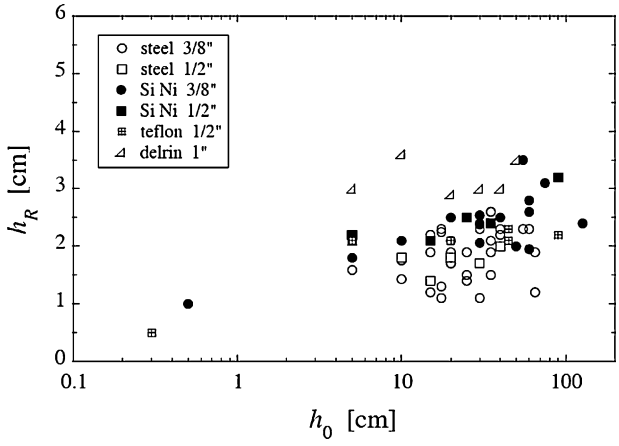

Fig. 6. The rebound height h_R as a function of the initial drop height h_0, for different spheres in our experiments.

The upward motion of the sphere into what is no longer a homogeneous fluid brings in additional effects, which due to the distribution of FIS may lead to less reproducibility of the motion; the observed oscillations of a falling sphere gave some indication of a random process [11]. We now have direct evidence of these structures from observations of bubbles entrained by the falling sphere in this experiment (see Appendix A).

All of these aspects play a role in decreasing the recoverable strain from the initial impact of the sphere. As a result there is a significant loss of kinetic energy; for instance in Fig. 2 the maximum rise velocity $u_R \sim 0.1$ m/s, which is much less than the impact velocity $U_0 \simeq 2.4$ m/s. This is also evident from the fact that the sphere remains in the fluid, whereas it started 30 cm above the surface. We have observed cases in which the sphere actually bounces back *out* of the fluid, but this is for a much higher concentration of surfactant and salt [44].

5. Surface deformation and cavity dynamics

The entry of a sphere into a viscous fluid typically forms a cavity of air by attaching to and distorting the free surface through which it passes [20,45]. For example, when a dry sphere sinks into a viscous oil, and the sphere surface is wetted more slowly than the sinking rate, a funnel shaped cavity is stretched out by the sphere, which pinches off within one diameter below the surface [19]. In our previous experimental study of wormlike micellar fluids, the sphere was held at the surface before release, so that the impact velocity was zero, and thus in principle $Fr = 0$ [18]. For viscoelastic fluids in this limit there is also a loss of symmetry which corresponds to the buckling of the elastic surface. In the experiments reported here, a similar smooth funnel shape is seen for the lighter spheres and the lower drop heights; similar shapes are seen in water (see e.g. [3]) and polymer fluids [23]. The pinch-off process for the smooth, viscous-like cavity in a wormlike micellar fluid is shown for a $d = 2.54$ cm delrin sphere in Fig. 7. The funnel shaped surface is narrowest somewhere above the sphere, and meets close to that point at pinch-off, resulting in a small entrained bubble (Fig. 7d), as seen previously for spheres with no initial velocity [18]. As the drop height is increased, changes are observed in the qualitative shape of the cavity, as shown in Fig. 8 for a $d = 0.95$ cm silicone nitride sphere. We note that in all of our experiments there was essentially no recoiling jet rising above the surface [20], in agreement with other experiments in polymers [21,22] and wormlike micellar fluids [32].

A shape instability of the smooth cavity shape is observed for higher h_0 (larger U_0), shown in Fig. 8b for a $d = 0.95$ cm silicon nitride sphere falling from $h_0 = 50$ cm. The cavity wall is no longer simply curved, but has an abruptly necked-down region above a curved bulbous shape. The entry velocity at which this transition occurs varies with the sphere mass and size. The detailed formation of this unusual cavity is shown in Fig. 9 for a $d = 0.95$ cm steel sphere falling from $h_0 = 30$ cm. The necking initially occurs approximately one diameter below the surface (Fig. 9a), as if the wall has failed locally, and the cavity begins to close there. As the sphere sinks further, the cavity bulges significantly just below this neck. It may be that a surface buckling has occurred, similar to that observed for a slowly stretched cavity behind a sinking sphere [18]. As the sphere advances deeper into the fluid, it draws out the bulbous cavity beneath the necking point (Fig. 9b and c). The cavity actually seals at a point closer to the sphere, and not at the narrower necked region above (Fig. 9d). In fact, this part at the surface seems resistant to pinch-off, and the large air bulb does not become an entrained bubble, but shrinks more or less in place as the air escapes through the neck (Fig. 9e).

The occurrence of this bulbous cavity below the neck suggests a change in the nature of the surface at this neck, evident in the widening of the air cavity just below. Two obvious candidates are the elasticity of the fluid and the surface tension. It is likely that the elasticity of the surface varies with depth, and that the more elastic surface is more resistant to pinch-off; a recent membrane model for a stretched viscoelastic surface indicates that the highest stretching occurs at the narrowest part of the cavity [19]. However this localized neck suggests that a specific change has occurred, perhaps a local strain hardening, as has been seen in filament experiments in other wormlike micellar fluids [38,46].

Another possible explanation for the observed change in surface at the neck would be to relate it to dynamic surface tension effects in micellar fluids [33]. As the sphere plunges into the fluid, it rapidly created new surface area, however the rate at which it does so decreases as the sphere slows down, and the whole process is abruptly interrupted when the cavity closes. To estimate the relevance of dynamic surface tension effects, we define a timescale t_R for the creation of new surface area [33,47]. The change in surface area for the approximately cylindrical cavity of diameter d is $\pi d U(z)$, where U is the speed of the sphere at depth z, and $U(0) = U_0$. From this we obtain $t_R \sim \pi d^2/\pi d U = d/U$. Typically the necking occurs around the

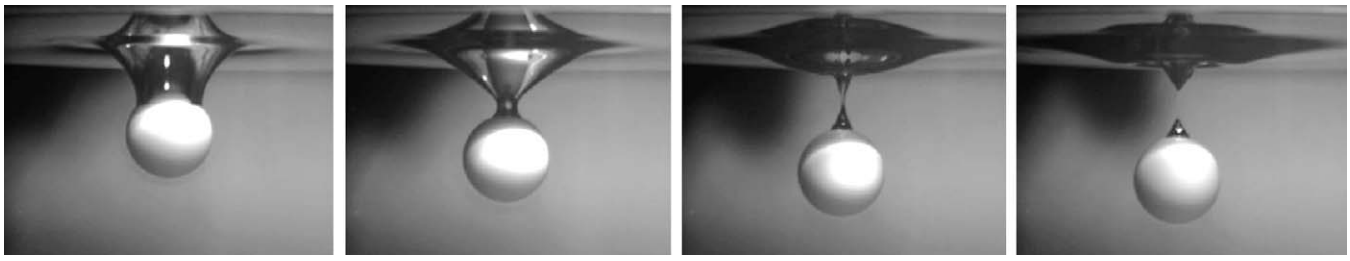

Fig. 7. Cavity formation for a $d = 2.54$ cm delrin sphere dropped from $h_0 = 5$ cm ($Re \simeq 0.58$, $De \simeq 78$; $Fe \simeq 16$), characteristic of the 'smooth' cavity surface state. The images shown are separated by 20 ms.

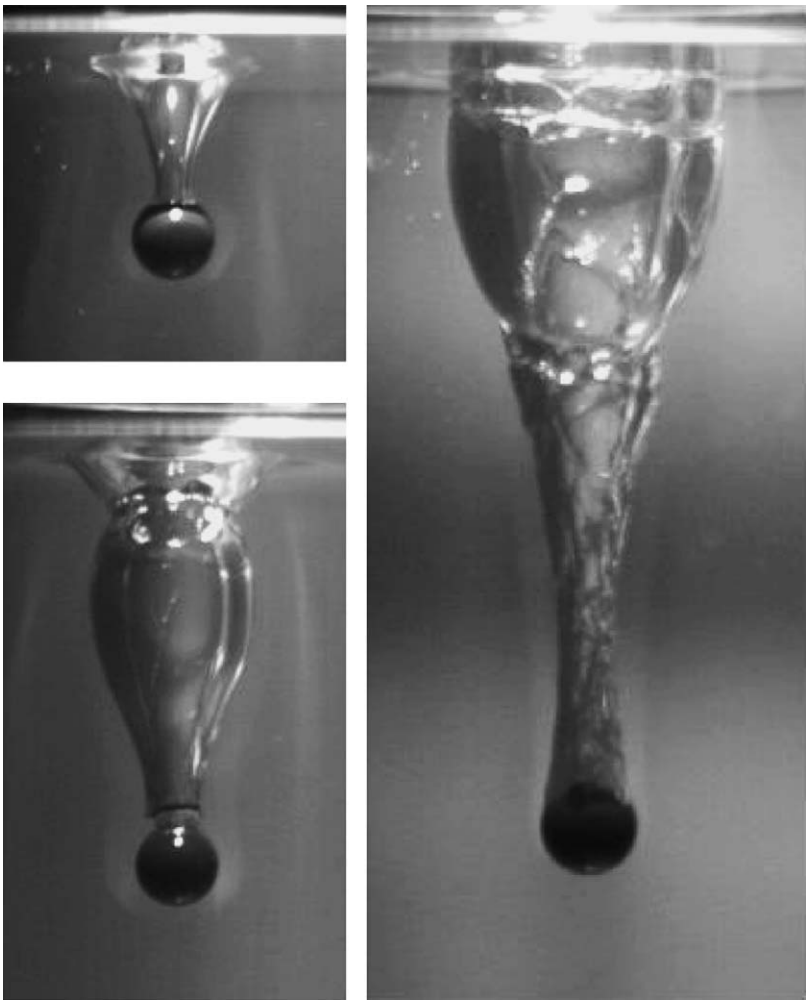

Fig. 8. Different cavity shapes produced by the impact of a $d = 0.95$ cm silicone nitride sphere on the free-surface of a wormlike micellar fluid ($\Omega = 9.3$) for: (a) $h_0 = 10$ cm, $De \simeq 300$, $Fe \simeq 200$; (b) $h_0 = 50$ cm, $De \simeq 660$, $Fe \simeq 1000$; (c) $h_0 = 127$ cm, $De \simeq 1050$, $Fe \simeq 2500$.

depth $z \simeq d$, and for these experiments $U(d) \simeq U_0$ (including the experiment shown in Fig. 9); this yields $t_R \sim d/U_0 \simeq 4$ ms. The crossover timescale seen by Cooper-White et al. was about 15 ms (for CTAB/NaSal), thus our observation seems inconclusive. However note that to connect the necking region with this crossover would suggest that the surface tension would be higher at the top, and lower as the sphere slows down, which would not explain the observation that the neck and the cavity above it remain open, while pinch-off occurs at the bottom. Another, related possibility would be that the sphere has collected surfactant near its surface, and then shed them at the neck, resulting in a much *lower* surface tension at that location. This would explain

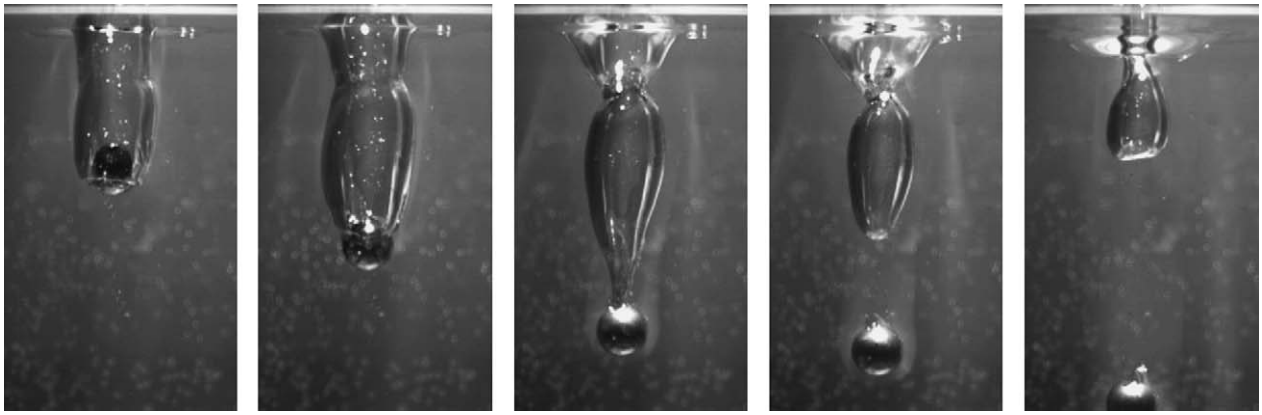

Fig. 9. Cavity dynamics for a $d = 0.95$ cm steel sphere, $h_0 = 30$ cm ($Re \simeq 0.53$, $De \simeq 510$; $Fe \simeq 1860$), shown after the moment of impact at t (a) 13 ms; (b) 21 ms; (c) 33 ms; (d) 37 ms; (e) 53 ms.

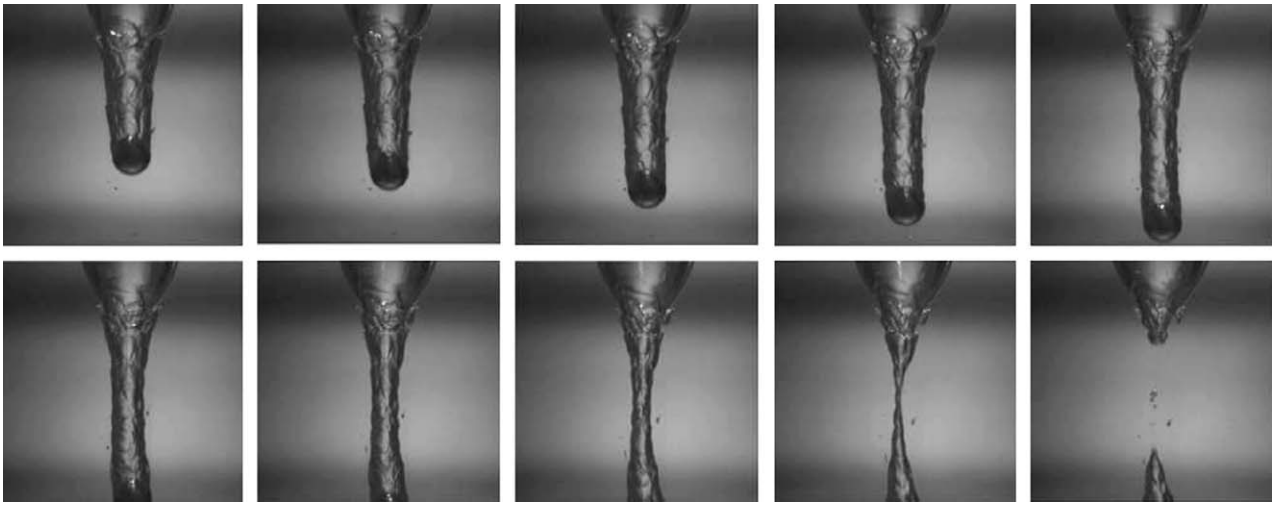

Fig. 10. Cavity dynamics for a $d = 0.95$ cm steel sphere dropped from $h_0 = 70$ cm, shown every 2.0 ms ($Re \simeq 0.82$, $De \simeq 780$; $Fe \simeq 4 \times 10^3$).

the persistance of the neck and its resistance to pinch-off. Further investigation of these possibilities should probably include modeling of flow past a sphere with a free surface which allows for surfactant gradients in the bulk and surface.

Fig. 8c shows the third qualitatively different cavity we have seen experimentally; for each sphere we studied, there is another critical impact velocity above which there is a transition in the cavity wall texture from smooth to rough. In Fig. 10, we show the cavity dynamics for a $d = 0.95$ cm steel sphere dropped from $h_0 = 70$ cm. This case corresponds to very large elastic effects: $De \simeq 780$, $Fe \simeq 4 \times 10^3$. However the flow is still viscous, with $Re \simeq 0.82$; note also that $Fr \simeq 140$. The texture of the cavity is initially smooth, but begins to show a structured roughness about one diameter below the initial surface. This apparent surface fracture in the cavity suggests that it is being torn as the sphere plunges into the fluid. Moreover, the scalloped structures seen in the surface texture are not stretched or pulled downward as the sphere continues to descend, as indicated in Fig. 11. The fact that identifiable features in the texture remain at a fixed depth indicates that the cavity surface is no longer being stretched. It may be that the sphere is sinking much faster that it can be wetted, and that there is an instability occurring at the contact line, where new interface is continuously being created, rather than stretching the pre-existing surface further. A closeup of the cavity surface where it meets the rapidly falling sphere (with a speed of 200 cm/s at a depth of 6 cm) is illustrated in Fig. 12, which shows that the contact line with the fluid is swept back to the rear half of the sphere. The hairlike fractures seen just behind the sphere, which sometimes have a characteristic scalloped shape (see Figs. 11 and 12) again hint at surface FIS, and

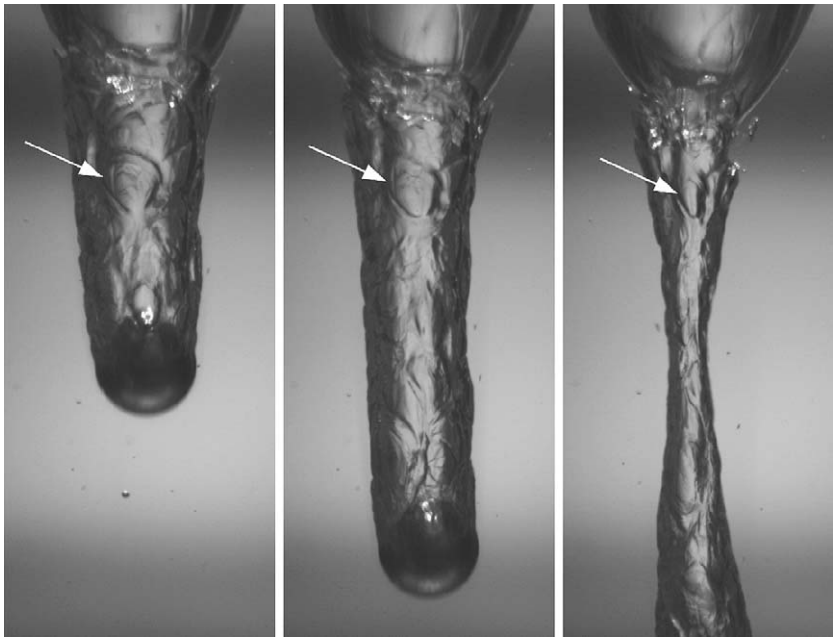

Fig. 11. Closeup of the development of surface texture in the cavity behind a $d = 0.95$ cm steel sphere dropped from $h_0 = 70$ cm ($Fe \simeq 4 \times 10^3$). The arrow indicates a scallop-shaped fracture which remains at the same depth while the sphere plunges downwards (frames shown are separated by 8 ms).

Fig. 12. Closeup of the surface where the micellar fluid meets a falling $d = 0.95$ cm steel sphere, in a different experiment than Figs. 10 and 11. The sphere was dropped from $h_0 = 70$ cm, and at the depth shown (about 6 cm below the surface) has an estimated speed of 200 cm/s ($Re \simeq 0.44$, $De \simeq 420$).

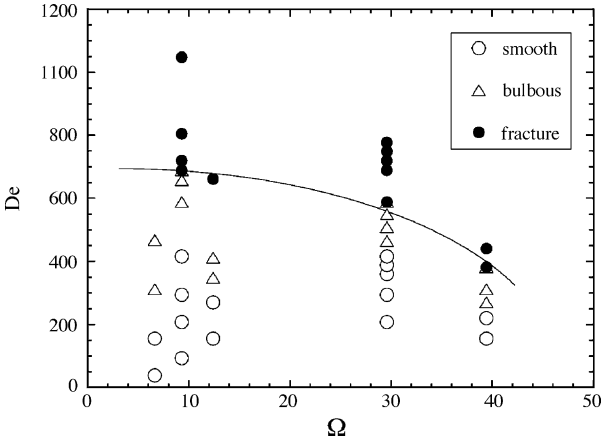

Fig. 13. Texture of the cavity surface for the experiments, shown as a function of Deborah number De and elastic Grashof number Ω (Eq. (2)).

bear some resemblance to the surface blistering seen in rapidly stretched wormlike micellar filaments [38].

It is natural to expect either a critical De or Fr value to determine the onset of this surface roughness. Our data indicates that this is approximately correct: the transition occurs in the range $De \sim 400$–700. Within this range, there is a systematic variation of the De value at onset with other aspects of the sphere, however neither a critical value of Fe nor a critical Wb condition [34] appears to characterize the transition. The elastic Froude number Fe defined in Eq. (1) is the product of Fr and another dimensionless parameter Ω, recently shown to be important in modeling stall in viscoelastic filament dynamics [38]:

$$\Omega = \frac{\Delta\rho g d}{G}. \tag{2}$$

This ratio is a sort of elastic Grashof number, in that it compares the buoyant force to opposing elastic forces, instead of opposing viscous forces [52]. In Fig. 13 we plot the dependence of the kind of surface shape observed on both De and Ω. For a given sphere, the increase in height results in a greater impact speed, and thus a larger De, whereas the gravitational force on the sphere remains the same. This force however does increase with either sphere size or density. The data in Fig. 13 shows that both the non-dimensional velocity (De) and force (Ω) are important to the onset of the surface tearing or fracturing. It is also apparent that the transition to tearing occurs at a slower speed (lower De) if a greater force (larger Ω) is applied. It is not clear what physical processes determine this transition, producing the rough, scalloped surface texture; perhaps a surface version of the well-known sudden filament failure in polymer fluids [51] or wormlike micellar fluids [38], or to the onset of FIS at the free surface, where high stress is known to concentrate in boundary layers [18,54,55].

Most of the dynamics of the sphere, such as the oscillations characterized by the penetration depth and rebound height, occur well after the cavity has sealed (see Fig. 1). Thus it is not surprising that the dependence of z_p and z_R on Fe are insensitive to the transition in cavity surface just discussed. However, we would expect some effect to be seen in the position below the surface at which the cavity eventually seals—the seal depth z_s. In Fig. 14 we plot z_s as a function of the drop height for two representative spheres in our study. In each case there seems

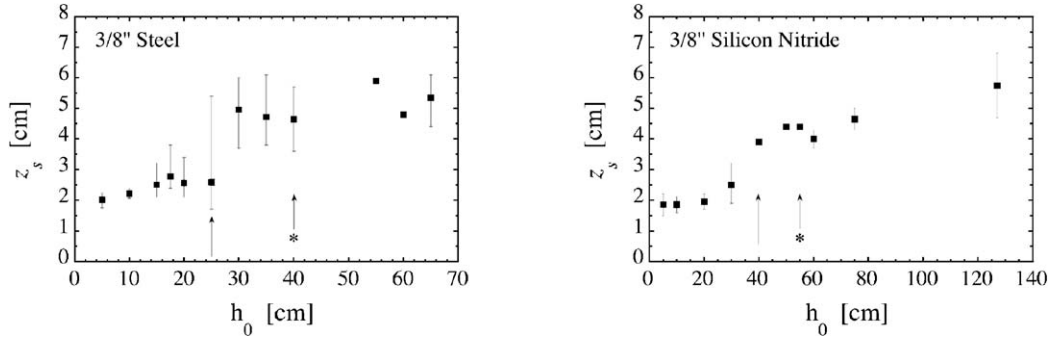

Fig. 14. Cavity seal depth z_s as a function of drop height h_0 for (a) $d = 0.95$ cm steel sphere; (b) $d = 0.95$ cm silicon nitride sphere. The error bars show the range of variation of the data.

to be a discontinuous increase in the seal depth occurring at a certain drop height (between 25 and 30 cm for Fig. 14a, and 30 and 40 cm for Fig. 14b); this is also true for the other spheres we have studied. The transition heights for the cavity surface are indicated by arrows: bulbous shape (plain, 25 and 40 cm, respectively) and rough shape (asterisks, 40 and 55 cm, respectively). Interestingly, the discontinuity seems to occur in tandem with the transition from smooth to bulbous shape, and *not* with the transition to a rough surface. This suggests that the lower speed transition many indeed be the beginning of a change in the response of the fluid surface to rapid stretching.

Within the precision of our data, it appears that the smooth surface has one value of z_s, which approximately doubles for the bulbous and rough surface regime. There seemed to be more variation in the seal depth in the rough regime as when the surface was smooth. This may be due to the sensitivity to variations in initial conditions, such as the drop height or the local distribution of micelles, which could strongly influence the point of pinch-off by affecting the creation of surface structure in the rough regime.

6. Discussion and conclusions

We have presented an experimental study of the impact of a rigid sphere falling into a particular viscoelastic fluid, a solution of 80/60 mM CPCl/NaSal, focusing on two main aspects: the transient motion of the sphere as it enters the fluid, and the dynamics of the rapidly stretched surface. There are significant differences between our experiments with this non-Newtonian fluid, and previous experiments with both Newtonian and polymeric fluids. Among these are the modified scaling parameters for the penetration depth, the 'elastic Froude number' *Fe*, which relates initial kinetic energy to the elastic modulus of the fluid. We first briefly discuss scaling exponents in fluid impact. If the sphere stops before the cavity closes, one could estimate the depth at which all initial kinetic energy would be consumed by the gravitational potential energy of a fluid column emptied by the sphere. Assuming that this fluid column is a cylinder of length z_p and diameter d, one obtains the scaling $z_p/d \sim Fr^{1/2}$. Inviscid arguments on the seal depth z_s also lead to a scaling with the Froude number: $z_s/d \sim Fr^{1/3}$ [43].

For the situation considered here, we can obtain the scaling for the penetration depth *a posteriori* by postulating that the sphere is stopped by the elasticity of the fluid, and balancing the initial kinetic energy of the sphere with the stored elastic energy at the moment it stops at a depth z_p. For linear materials the elastic energy stored in a deformed volume V is given by $G\epsilon^2 V$, where ϵ is some measure of the deformation. Using birefringence techniques to visualize the stress field, observations of sphere impact into micellar fluids indicate that the elastic deformation immediately after impact covers a large region around the sphere, and that the relevant length scale is the depth of the sphere itself [44]. Thus we estimate $V \sim z_p^3$, and $\epsilon \sim z_p/z_p \sim \mathrm{O}(1)$. Due to the rapidity of the impact we include the rate dependence in the elasticity from the storage modulus G' of the fluid: we use $G = G'(\dot\gamma)$ with $\dot\gamma \sim U/d$ as an estimate of the shear rate at the moment of impact. As the measured storage modulus of our fluid is reasonably close to the formula from the Maxwell model [38], we use this analytic relation in our estimate of the energy balance [48]:

$$\rho_s d^3 U_0^2 \sim G'\epsilon^2 V = \frac{G_0\lambda^2 U_0^2/d^2}{1+\lambda^2 U_0^2/d^2}\, z_p^3, \tag{3}$$

where d is the diameter and ρ_s is the density of the sphere. Simplifying and rearranging into non-dimensional parameters, we obtain the theoretical scaling

$$\frac{z_p}{d} \sim Fe^{1/3}\left(\frac{1+De^2}{De^2}\right)^{1/3}. \tag{4}$$

For $De^2 \gg 1$, which corresponds to most of our experiments (see Table 1), this leads to the observed scaling $z_p/d \sim Fe^{1/3}$.

There is an intriguing connection between the scaling we observe for the penetration depth, which is the point at which the sphere is initially stopped by the micellar fluid, and similar measurements in granular materials [24,27,49,50]. In our experiments, the sphere is initially stopped as it enters the fluid, and bounces back one or more times before it reaches a state of steady sedimentation. Our data suggest that this initial impact dynamics depends on the ratio of kinetic energy to elasticity (the dimensionless parameter *Fe*), and not the Froude number as is the case for Newtonian fluids. Interestingly, experiments performed on sphere impact in granular materials, including crater formation [27,49,50] and granular jets [24] also indicate that something different than *Fr* is needed to rescale their data, due essentially to stress propagation through granular force chains [26].

More specifically, the measurement of the "stopping depth" for the impact of a sphere on a granular material has been found to have a scaling relationship with the height from which it was dropped; here we adapt the measurements reported elsewhere to our notation. Durian and coworkers have found that $z_p \sim h_0^{1/3}$ for spherical [49] and non-spherical projectiles [53]. A different scaling $z_p \sim h_0^{0.25}$ was found by Walsh et al. [50]. Given the scaling of the elastic Froude number $Fe \sim U_0^2$, and the free-fall relation $U_0^2 = 2gh_0$, our observation of $z_p \sim Fe^{1/3}$ is consistent with the 1/3 scaling seen for granular materials. However our scaling also implies $z_p \sim \rho_s^{1/3}$, whereas for granular impact $z_p \sim \rho_s^{1/2}$ [49,53]. It remains to be seen if this common exponent is indicative of a common mechanism; further exploration is needed. It might also be fruitful to connect the material dependence of the other aspects of crater formation in granular systems to the cavity dynamics of viscoelastic fluids such as those reported here.

We have also seen transitions in the character of the cavity surface formed during penetration of the sphere, dependent on both the relaxation time (*De*) and the ratio of gravity to elasticity (the 'elastic Grashof number' Ω). We have observed two regimes of behavior: the smooth pinch-off as seen in viscous Newtonian and polymeric fluids, and a surface fracture at large velocities. It is tempting to ascribe a standard, polymer-like stretching dynamic to the upper, smooth surface, and a micellar-related breaking below the neck—the breaking of the micellar tubes which comprise

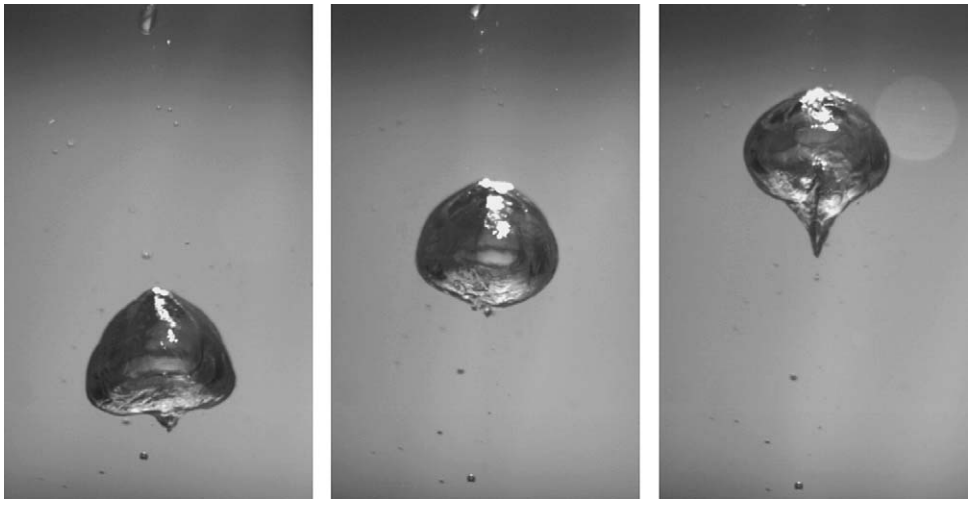

Fig. 15. After the impact of a $d = 1.27$ cm steel sphere falling from $h_0 = 70$ cm, a large air bubble (about 2 cm^3) entrained by the sphere rises through the fluid. The images are separated by $\Delta t = 33$ ms.

these fluids is well known [17], and has been suggested as the root of other hydrodynamic instabilities [11,16,38]. While we have not yet obtained direct evidence for this, our observations suggest that a sort of material fracture is occurring with increasing h_0. What remains to be done is to show directly a causal relationship with the micellar nature of the fluid, by searching for a similar instability in the impact on a polymer fluid surface (for a recent review of rupturing instabilities in stretched polymer flows, see [51]). So far as we know, this is the first observation of such a velocity-dependent transition from smooth to rough surface texture in the impact dynamics on a viscoelastic fluid.

Acknowledgments

We would like to thank R.H. (Bob) Geist for experimental assistance, F. Costanzo, T. Grumstrup, N.Z. Handzy, C. Misbah, M.C. Sostarecz, and B. Tilley for helpful comments and discussions, and H.A. Stone for helping to clarify our thinking on the elastic energy scaling. AB acknowledges support from the National Science Foundation (CAREER Award DMR-0094167).

Appendix A

Here we briefly report on observations made in the extreme cases of the sphere impact experiments described above: the entrainment of air into the micellar fluid. In many of the high *Fe* (high *Fr*) cases discussed above, a significant amount of air was entrained behind the falling sphere; this air would subsequently rise through the micellar fluid. An example of such a bubble is shown in Fig. 15, for a $d = 1.27$ cm steel sphere dropped from $h_0 = 70$ cm. With an estimated volume of about 2 cm^3, this bubble is significantly larger than the previous experiments on rising bubbles in wormlike micellar fluids [15,16].

However, of greater importance is the fact that the bubble is not at all rising into a relaxed, homogeneous fluid (as is usually studied), but instead moves into the wake of the sphere responsible for its entrainment. The result is that the bubble does not have a perfectly smooth surface as it rises, giving the appearance of crinkled aluminum foil. It also has an unusual shape, displaying at times an almost pointed leading edge, which may be due to the highly oriented wormlike micelles through which it is rising—this orientation is evident in the birefringence seen in the wake of such fluids, see [12,16]. Recently, similar forward-pointed bubbles were seen numerically in a two-dimensional geometry of an axially oriented nematic liquid crystal.[3] We expect a similar explanation here: that the flow-induced structures in the wake of the sphere [11] lead to a local micellar orientation which produces this pointed shape. Note that the bubble does also have a trailing edge cusp-like tail, as is seen in polymer fluids [56], and in fact jumps as it rises, as smaller bubbles do in wormlike micellar fluids [15,16].

References

[1] G. Birkhoff, E.H. Zarantonello, Jets, Wakes, and Cavities, Academic Press, New York, 1957.
[2] J.W. Glasheen, T.A. McMahon, Vertical water entry of disks at low Froude numbers, Phys. Fluids 8 (1996) 2078–2083.
[3] A. Mallock, Sounds produced by drops falling on water, Proc. Roy. Soc. London, Ser. A 95 (1918) 138–143.
[4] A. Prosperetti, H.N. Oğuz, The impact of drops on liquid surfaces and the underwater noise of rain, Annu. Rev. Fluid Mech. 25 (1993) 577–602.
[5] E.G. Richardson, The impact of a solid on a liquid surface, Proc. Phys. Soc. 61 (1948) 352–367.
[6] S. Gaudet, Numerical simulation of circular disks entering the free surface of a fluid, Phys. Fluids 10 (1998) 2489–2499.
[7] M. Lee, R.G. Longoria, D.E. Wilson, Cavity dynamics in high-speed water entry, Phys. Fluids 9 (1997) 540–550.
[8] R. Clift, J.R. Grace, M.E. Weber, Bubbles, Drops, and Particles, Academic Press, New York, 1978.
[9] R.P. Chhabra, Bubbles, Drops, and Particles in Non-Newtonian Fluids, CRC Press, Boca Raton, 1993.
[10] M. Arigo, G.H. McKinley, The effects of viscoelasticity on the transient motion of a sphere in a shear-thinning fluid, J. Rheol. 41 (1997) 103–128.

[3] J.J. Feng, private communication

[11] A. Jayaraman, A. Belmonte, Oscillations of a solid sphere falling through a wormlike micellar fluid, Phys. Rev. E 67 (2003) 65301–65304.
[12] S. Chen, J.P. Rothstein, Flow of a wormlike micelle solution past a falling sphere, J. Non-Newtonian Fluid Mech. 116 (2004) 205–234.
[13] A.M. Mollinger, E.C. Cornelissen, B.H.A.A. van den Brule, An unexpected phenomenon observed in particle settling: oscillating falling spheres, J. Non-Newtonian Fluid Mech. 86 (1999) 389–393.
[14] P. Weidman, B. Roberts, S. Eisen, in: V.D. Shalfeev (Ed.), Progress in Nonlinear Science, Proceedings III, Nizhny Novgorod, Novgorod, 2002.
[15] A. Belmonte, Self-oscillations of a cusped bubble rising through a micellar fluid, Rheol. Acta 39 (2000) 554–559.
[16] N.Z. Handzy, A. Belmonte, Oscillatory rise of a bubble in wormlike micellar fluids with different microstructures, Phys. Rev. Lett. 92 (2004) 124501–124504.
[17] M.E. Cates, S.J. Candau, Statics and dynamics of worm-like surfactant micelles, J. Phys.: Condens. Matter 2 (1990) 6869–6892.
[18] T. Podgorski, A. Belmonte, Surface folds during the penetration of a viscoelastic fluid by a sphere, J. Fluid Mech. 460 (2002) 337–348.
[19] T. Podgorski, A. Belmonte, Surface folding of viscoelastic fluids: finite elasticity membrane model, Eur. J. Appl. Math. 15 (2004) 385–408.
[20] A. Worthington, A Study of Splashes, Longman & Green, London, 1908.
[21] J.-M. Cheny, K. Walters, Extravagant viscoelastic effects in the Worthington jet experiment, J. Non-Newtonian Fluid Mech. 67 (1996) 125–135.
[22] J.-M. Cheny, K. Walters, Rheological influences on the splashing experiment, J. Non-Newtonian Fluid Mech. 86 (1999) 185–210.
[23] S. Nigen, K. Walters, On the two-dimensional splashing experiment for Newtonian and slightly elastic liquids, J. Non-Newtonian Fluid Mech. 97 (2001) 233–250.
[24] S.T. Thoroddsen, A.Q. Shen, Granular jets, Phys. Fluids 13 (2001) 4–6.
[25] R. Mikkelsen, M. Versluis, E. Koene, G.-W. Bruggert, D. van der Meer, K. van der Weele, D. Lohse, Granular eruptions: void collapse and jet formation, Phys. Fluids 14 (2002) S14.
[26] M.P. Ciamarra, A.H. Lara, A.T. Lee, D.I. Goldman, I. Vishik, H.L. Swinney, Dynamics of drag and force distributions for projectile impact in granular medium, Phys. Rev. Lett. 92 (2004) 194301–194304.
[27] J.R. de Bruyn, A.M. Walsh, Penetration of spheres into loose granular media, Can. J. Phys. 82 (2004) 439–446.
[28] A.N. Srdic-Mitrovic, N.A. Mohamed, H.J.S. Fernando, Gravitational settling of particles through density interfaces, J. Fluid Mech. 381 (1999) 175–185.
[29] N. Abaid, D. Adalsteinsson, A. Agyapong, R.M. McLaughlin, An internal splash: levitation of falling spheres in stratified fluids, Phys. Fluids 16 (2004) 1567–1580.
[30] L.-J. Leng, Splash formation by spherical drops, J. Fluid Mech. 427 (2001) 73–105.
[31] B. Kersten, C.D. Ohl, A. Prosperetti, Transient impact of a liquid column on a miscible liquid surface, Phys. Fluids 15 (2003) 821–824.
[32] F. Yang, Y. Qi, W. Morales, D.J. Hart, J.L. Zakin, Effect of surfactant additive composition on Worthington jet splashing, in: Proceedings of the 13th International Congress on Rheology, vol. 2, Cambridge, UK, 2000, p. 274.
[33] J.J. Cooper-White, R. Crooks, D.V. Boger, A drop impact study of wormlike viscoelastic surfactant solutions, Colloid Surf. A 210 (2002) 105–123.
[34] J. Lampe, R. DiLalla, J. Grimaldi, J.P. Rothstein, Impact dynamics of drops on thin films of viscoelastic wormlike micelle solutions, J. Non-Newtonian Fluid Mech. 125 (2005) 11–23.
[35] H. Rehage, H. Hoffmann, Viscoelastic surfactant solutions—model systems for rheological research, Mol. Phys. 74 (1991) 933–973.
[36] J.-F. Berret, D.C. Roux, G. Porte, Isotropic-to-nematic transition in wormlike micelles under shear, J. Phys. II 4 (1994) 1261–1279.
[37] C. Grand, J. Arrault, M.E. Cates, Slow transients and metastability in wormlike micelle rheology, J. Phys. II 7 (1997) 1071–1086.
[38] L.B. Smolka, A. Belmonte, Drop pinch-off and filament dynamics of wormlike micellar fluids, J. Non-Newtonian Fluid Mech. 115 (2003) 1–25.
[39] D.S. Ambwani, T. Fort, in: R.J. Good, R.R. Stromberg (Eds.), Surface and Colloid Science, vol. 11: Experimental Methods, 2nd ed., Plenum Press, New York, 1979, pp. 93–118.
[40] A.N. Mouchacca, D.E. Langberg, M. Nilmani, Characterization of phenomena associated with impacting spheres into glycerol solutions, Powder Tech. 88 (1996) 95–99.
[41] G.H. McKinley, R.P. Chhabra, D. De Kee (Eds.), Transport Processes in Bubbles, Drops, and Particles, 2nd ed., Taylor & Francis, London, 2001.
[42] D.D. Joseph, Fluid Dynamics of Viscoelastic Flows, Springer-Verlag, New York, 1990.
[43] H.N. Oğuz, A. Prosperetti, A.R. Kolaini, Air entrapment by a falling water mass, J. Fluid Mech. 294 (1995) 181–207.
[44] A. Belmonte, J.R. Gladden, Motion of spheres and cylinders through viscoelastic micellar fluids, (2006), in press.
[45] A. May, Vertical entry of missiles into water, J. Appl. Phys. 23 (1952) 1362–1372.
[46] J. Rothstein, Transient extensional rheology of wormlike micelle solutions, J. Rheol. 47 (2003) 1227.
[47] N. Mourougou-Candoni, B. Prunet-Foch, F. Legay, M. Vignes-Adler, K. Wong, Influence of dynamic surface tension on the spreading of surfactant solution droplets impacting onto a low-surface-energy solid substrate, J. Colloid Interf. Sci. 192 (1997) 129–141.
[48] R. Bird, R. Armstrong, O. Hassager, Dynamics of Polymeric Liquids, 2nd ed., Wiley and Sons, New York, 1987.
[49] J.S. Uehara, M.A. Ambroso, R.P. Ojha, D.J. Durian, Low-speed impact craters in loose granular media, Phys. Rev. Lett. 90 (2003) 194301–194304.
[50] A.M. Walsh, K.E. Holloway, P. Habdas, J.R. de Bruyn, Morphology and scaling of impact craters in granular media, Phys. Rev. Lett. 91 (2003) 104301–104304.
[51] Y.M. Joshi, M.M. Denn, Rupture of entangled polymeric liquids in elongational flow, J. Rheol. 47 (2003) 291–298.
[52] D.J. Tritton, Physical Fluid Dynamics, Oxford University Press, Oxford, 1988.
[53] K.A. Newhall, D.J. Durian, Projectile-shape dependence of impact craters in loose granular media, Phys. Rev. E 68 (2003) 60301–60304.
[54] H.K. Rasmussen, O. Hassager, Three-dimensional simulations of viscoelastic instability in polymeric filaments, J. Non-Newtonian Fluid Mech. 82 (1999) 189–202.
[55] M. Yao, G.H. McKinley, Numerical simulations of extensional deformations of viscoelastic liquid bridges in filament stretching devices, J. Non-Newtonian Fluid Mech. 74 (1998) 47–88.
[56] Y. Liu, T. Liao, D.D. Joseph, A two-dimensional cusp at the trailing edge of an air bubble rising in a viscoelastic liquid, J. Fluid Mech. 304 (1995) 321–342.